Hindawi Publishing Corporation
Journal of Nanomaterials
Volume 2014, Article ID 240346, 7 pages
http://dx.doi.org/10.1155/2014/240346

Research Article

Anodic Fabrication of Ti-Nb-Zr-O Nanotube Arrays

Qiang Liu,[1] Dongyan Ding,[1] and Congqin Ning[2]

[1] *Institute of Microelectronic Materials and Technology, School of Materials Science and Engineering, Shanghai Jiao Tong University, Shanghai 200240, China*
[2] *State Key Laboratory of High Performance Ceramics and Superfine Microstructure, Shanghai Institute of Ceramics, Chinese Academy of Sciences, Shanghai 200050, China*

Correspondence should be addressed to Dongyan Ding; dyding@sjtu.edu.cn

Received 14 December 2013; Revised 1 March 2014; Accepted 1 March 2014; Published 27 March 2014

Academic Editor: Amirkianoosh Kiani

Highly ordered Ti-Nb-Zr-O nanotube arrays were fabricated through pulse anodic oxidation of Ti-Nb-Zr alloy in 1 M NaH_2PO_4 containing 0.5 wt% HF electrolytes. The effect of anodization parameters and Zr content on the microstructure and composition of Ti-Nb-Zr-O nanotubes was investigated using a scanning electron microscope equipped with energy dispersive X-ray analysis. It was found that length of the Ti-Nb-Zr-O nanotubes increased with increase of Zr contents. The diameter and the length of Ti-Nb-Zr-O nanotubes could be controlled by pulse voltage. XRD analysis of Ti-Nb-Zr-O samples annealed at 500°C in air indicated that the (101) diffraction peaks shifted from 25.78° to 25.05° for annealed Ti-Nb-Zr-O samples with different Zr contents because of larger lattice parameter of Ti-Nb-Zr-O compared to that of undoped TiO_2.

1. Introduction

Nanostructures of different metals or semiconductors have received much attention due to the wide application of these materials in photocatalysts, solar energy conversion, gas sensing, and biomedical applications [1–4]. TiO_2 nanotubes have been widely investigated due to their excellent biomedical application and photocatalytic effect since 1972 [5]. However, TiO_2 can be only excited by UV light which only occupies 5% of the solar spectrum because of its wide band gap (3.2 eV). Therefore, many approaches were used to extend the spectral response of the titanium dioxide to the visible light region and impurity doping is one of the typical and effective approaches. Many metal elements (Fe, Mo, Cr, Nb, etc.) and nonmetal elements (B, C, N, S, and F) have been used to dope TiO_2 to broaden its application fields [6–8]. Zr and Nb doping could affect the optical absorption ability of TiO_2 oxide. Hirano et al. reported that the onset of absorption of TiO_2 shifted to longer wavelengths by Zr and Nb doping [9, 10].

One-dimensional nanostructures have advantages over films and powder because the former can provide large surface-to-volume ratio and unidirectional electrical channel. Several research groups have reported the anodic formation of oxide nanostructures on the surfaces of titanium alloys to achieve good photocatalysts, solar energy conversion, gas sensing, and biomedical applications. Numerous methods have been reported for fabricating TiO_2 nanotubes including template-assisted process [11], hydrothermal reaction [12], seed growth [13], and anodization methods [14].

Anodic oxidation technique is relatively a simple method to fabricate one-dimensional nanotubes in comparison with other methods. Allam et al. reported the fabrication of Ti-Pd mixed oxynitride nanotube arrays through anodization of Ti-Pd alloy [15]. Berger et al. reported on the fabrication of Ti-Al-O nanotubes through anodization of Ti-Al alloys [16]. Nb- and Zr-doped TiO_2 nanotubes were also investigated recently. Liu et al. fabricated Ti-Nb-O nanotubes on Ti35Nb alloy and found that Nb-doped TiO_2 nanostructures had excellent hydrogen sensing capability [17]. Allam et al. fabricated Ti-Nb-Zr-O nanotubes through anodization of Ti35Nb5Zr alloy for enhanced hydrogen generation by water photoelectrolysis [18]. Li et al. found that the Nb- and Zr-doped TiO_2 nanostructures showed good biological properties [19].

To date, rare work has been reported on the effect of Zr content on the formation of Ti-Nb-Zr-O nanotubes. In

the present work, we fabricated highly ordered Ti-Nb-Zr-O nanotube arrays on Ti-Nb-Zr alloy substrate with different Zr contents by pulse anodic oxidation. The effect of Zr content and anodization parameters on the microstructures of Ti-Nb-Zr-O oxides was investigated.

2. Experiment Section

2.1. Synthesis of Ti-Nb-Zr-O Nanotubes. Prior to anodization, all of the Ti-Nb-Zr alloy samples (Ti35Nb5Zr, Ti35Nb10Zr, Ti35Nb15Zr) were ground and polished with number 2000 SiC emery papers and then ultrasonically cleaned with absolute alcohol. Finally, they were rinsed with deionized water and dried in N_2 stream. Electrochemical anodization was carried out with a pulse voltage stabilizer. Anodic samples were fabricated with pulse voltages of 20 V, 30 V, and 40 V with a constant frequency of 4000 Hz and duty cycle of 20% for 90 minutes in electrolytes of 1 M NaH_2PO_4 containing 0.5 wt% HF. The pulse frequency varied from 2000 Hz to 4000 Hz. The effects of anodization voltage and pulse frequency on the microstructures and composition of Ti-Nb-Zr-O samples with different Zr contents were investigated.

2.2. Microstructural Characterization. The structure morphology and composition of Ti-Nb-Zr-O samples were investigated using a scanning electron microscope (SEM; FEI SIRION 200, USA) equipped with energy dispersive X-ray analysis (EDXA; OXFORD INCA, USA). The as-anodized Ti-Nb-Zr-O samples grown on different Ti-Nb-Zr alloy substrates were annealed at 500°C in air. Phase structures of the as-annealed Ti-Nb-Zr-O samples were characterized with X-ray diffraction (XRD, D/max 2550 V). For reference, undoped TiO_2 nanotubes were also fabricated through anodization of pure Ti substrate.

3. Results and Discussion

Figure 1 shows top and cross-section views of Ti-Nb-Zr-O nanotubes grown on Ti35Nb5Zr alloy substrate at different voltages. The oxide sample prepared at 20 V showed a web-like structure rather than a nanotubular array morphology. When the anodization voltage increased to 30 V, the nanotube arrays could form. The average diameter and length of the nanotubes were 170 nm and 4.75 μm, respectively. When the anodization voltage increased to 40 V, the average diameter and length of the nanotubes were 220 nm and 4.8 μm, respectively. The slight increase in length from about 4.75 μm to 4.8 μm was attributed to a competition between an electrochemical oxide formation and chemical dissolution of oxide by fluoride ions. The formation rate of the nanotube bottom and the dissolution rate of the nanotube top at an anodization voltage of 30 V were almost equivalent. Therefore, the length of the nanotubes almost remained unchanged when the anodization voltage increased to 40 V.

Figure 2 shows top and cross-section views of Ti-Nb-Zr-O nanotubes grown on Ti35Nb10Zr alloy substrate at different voltages. When the anodization voltage was 20 V, the as-grown Ti-Nb-Zr-O nanotube arrays had a clear nanotubular morphology. When the anodization voltage increased to 30 V, the average diameter and length were 150 nm and 5.25 μm, respectively. At 40 V, Ti-Nb-Zr-O nanotube arrays grown on the Ti35Nb10Zr alloy substrate had an average diameter of 206 nm and average length of 6.12 μm. The diameter was slightly smaller than that of the nanotubes grown on Ti35Nb5Zr alloy substrate.

Figure 3 shows top and cross-section views of Ti-Nb-Zr-O nanotubes grown on Ti35Nb15Zr alloy substrate at different voltages. The average length of the Ti-Nb-Zr-O nanotubes was 8.13 μm when the anodic voltage was 40 V. Summary of the nanotube length and diameter of the three kinds of nanotubes is shown in Table 1.

Table 1: Summary of average length and diameter of the nanotubes grown at different anodization voltages.

Samples	Anodization voltage	Average length (μm)	Average diameter (nm)
Ti35Nb5Zr	20 V	—	—
	30 V	4.75	170
	40 V	4.80	220
Ti35Nb10Zr	20 V	2.26	98
	30 V	5.23	150
	40 V	6.12	206
Ti35Nb15Zr	20 V	3.25	103
	30 V	5.84	153
	40 V	8.13	210

During the anodization process, many factors such as oxidation electrolyte, anodization voltage, and time could affect the formation of Ti-Nb-Zr-O nanotubes. There is a competition between the electrochemical oxide formation and chemical dissolution of oxide by fluoride ions. The nanotube growth could reach a steady state in which the formation rate at the bottom and dissolution rate at the top are equal [20]. The growth of Ti-Nb-Zr-O nanotubes remarkably depended on local electric field and solution diffusion rate and took place preferentially at some locations on the Ti-Nb-Zr alloy substrate. The anodic formation mechanism of the Ti-Nb-Zr-O nanotubes can be represented as follows [21, 22]:

$$X + 2H_2O \longrightarrow XO_2 + 4H^+ + 4e^- \quad [X = Ti, Zr] \tag{1}$$

$$XO_2 + 4H^+ + 6F^- \longrightarrow [XF_6]^{2-} + 2H_2O \tag{2}$$

$$2Nb + 5H_2O \longrightarrow Nb_2O_5 + 10H^+ + 10e^- \tag{3}$$

$$Nb_2O_5 + 10H^+ + 14F^- \longrightarrow 2[NbF_7]^{2-} + 5H_2O \tag{4}$$

At first, oxidized metal species react with O^{2-} ions (from H_2O) to form an oxide layer growth on the metal surface. In contrast, due to the presence of F^- ions, dissolution and breakdown of oxide layer occur along random path through this layer and form disordered wormlike structure. The oxide layer will be finally removed by chemical dissolution and water-soluble $[XF_6]^{2-}$ or $[NbF_7]^{2-}$ formed, making the underneath highly ordered tube structure observable from

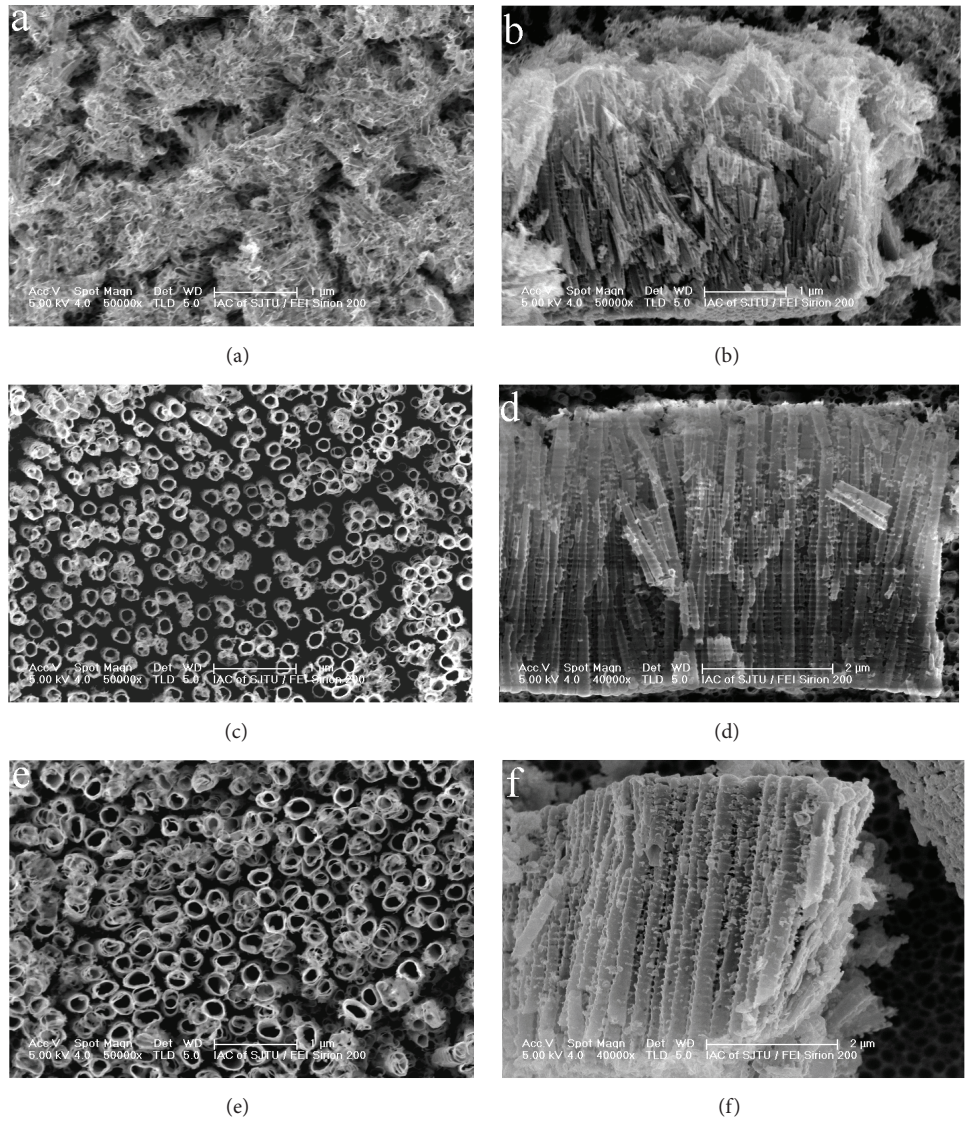

Figure 1: Top and cross-section views of Ti-Nb-Zr-O nanotubes grown on Ti35Nb5Zr alloy substrate at different voltages with a constant frequency of 4000 Hz and duty cycle of 20% for 90 minutes, (a)-(b) 20 V, (c)-(d) 30 V, and (e)-(f) 40 V.

Table 2: EDS analysis of the Ti-Nb-Zr-O nanotubes grown on different Ti-Nb-Zr alloy substrates at 40 V with a constant frequency of 4000 Hz and duty cycle of 20% for 90 minutes.

Samples	Ti (wt%)/(at%)	O (wt%)/(at%)	Nb (wt%)/(at%)	Zr (wt%)/(at%)
Ti35Nb5Zr	28.94/16.05	46.27/76.84	21.54/6.16	3.25/0.95
Ti35Nb10Zr	28.25/16.13	44.30/75.75	21.00/6.19	6.45/1.94
Ti35Nb15Zr	26.25/15.58	42.92/74.66	21.89/6.70	9.85/3.07

the top. Meanwhile, oxidized metal species could react with O^{2-} ions to form a new oxide layer. When the formation rate of the nanotube bottom and the dissolution rate of the nanotube top are equivalent, the length of nanotube remains unchanged. For the Ti-Nb-Zr alloy an increase in anodization voltage could increase the nanotube length since the driving force for ionic transport through the barrier layer at the pore bottom could be enhanced, which will result in faster migration of cations and/or anions and thus movement of the Ti-Nb-Zr/Ti-Nb-Zr-O interface into the Ti-Nb-Zr alloy.

Our experimental results revealed that Zr content in the Ti-Nb-Zr alloy played an important role in formation of Ti-Nb-Zr-O nanotubes because of different electrochemical properties of Ti and Zr elements. The solubility of the fluoride complex for $[ZrF_6]^{2-}$ is larger than that for $[TiF_6]^{2-}$. This could result in a larger anodic current for the Ti-Nb-Zr alloy

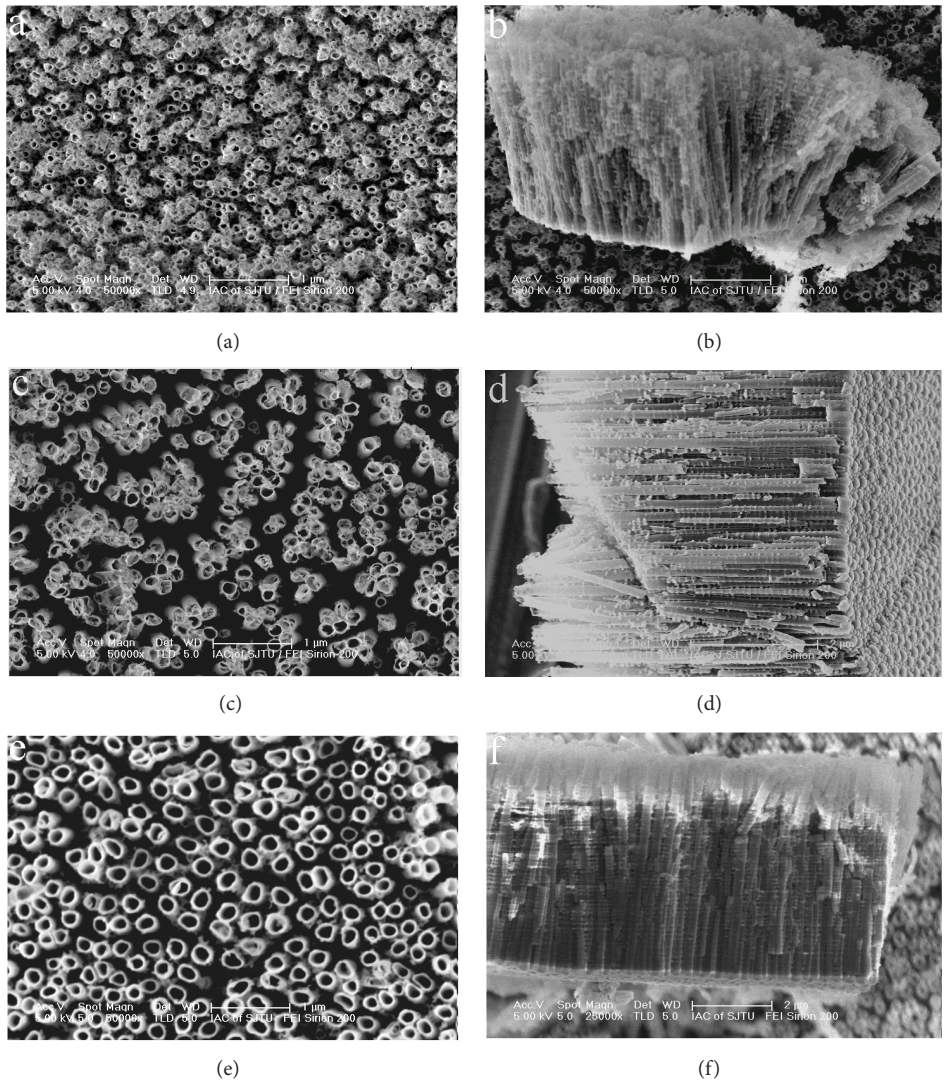

Figure 2: Top and cross-section views of Ti-Nb-Zr-O nanotubes grown on Ti35Nb10Zr alloy substrate at different voltages with a constant frequency of 4000 Hz and duty cycle of 20% for 90 minutes, (a)-(b) 20 V, (c)-(d) 30 V, and (e)-(f) 40 V.

with higher Zr content than that with lower Zr content at the same potential [21, 23]. The dissolution rate of the as-formed oxide layers by fluoride ion should be another factor in determining the length of the Ti-Nb-Zr-O nanotubes [24]. As shown above, the formation of Ti-Nb-Zr-O nanotubes with a high Zr content was easier than that with a low Zr content.

EDS analyses of the as-anodized Ti-Nb-Zr-O samples with different Zr contents were carried out to investigate the composition of the Ti-Nb-Zr-O samples. As shown in Table 2, each sample was mainly composed of Ti, Nb, Zr, and O elements. With the increase of Zr content of original alloys, contents of the Ti and Zr elements in the Ti-Nb-Zr-O oxide layer also changed correspondingly. The contents of Nb and Zr elements in the Ti-Nb-Zr-O samples were smaller than those of the original alloys. This phenomenon may be explained by considering the difference in the dissolution rate for different oxide systems since previous reports have shown that the nanotube formation on different pure metals had different chemical dissolution rates in the dilute HF electrolytes [25].

The effect of pulse frequency on the formation of Ti-Nb-Zr-O nanotubes was also investigated. Figure 4 shows SEM images of the Ti-Nb-Zr-O samples fabricated at 40 V with a constant frequency of 2000 Hz and duty cycle of 20% for 90 minutes on different Ti-Nb-Zr alloy substrates. As shown in Figure 4(a), the top surface of the oxide layer had a lot of irregular nanoporous structures and high aligned nanotube arrays did not form due to a low electrical field. However, the nanotube structure grown on Ti35Nb10Zr alloy substrate became denser and more vertically oriented at the same condition. Furthermore, the nanotubes grown on Ti35Nb15Zr alloy substrate presented a much more regular, well-aligned nanotube array architecture. This proved that the Ti35Nb15Zr system was easier for nanotube growth than the Ti35Nb5Zr system did.

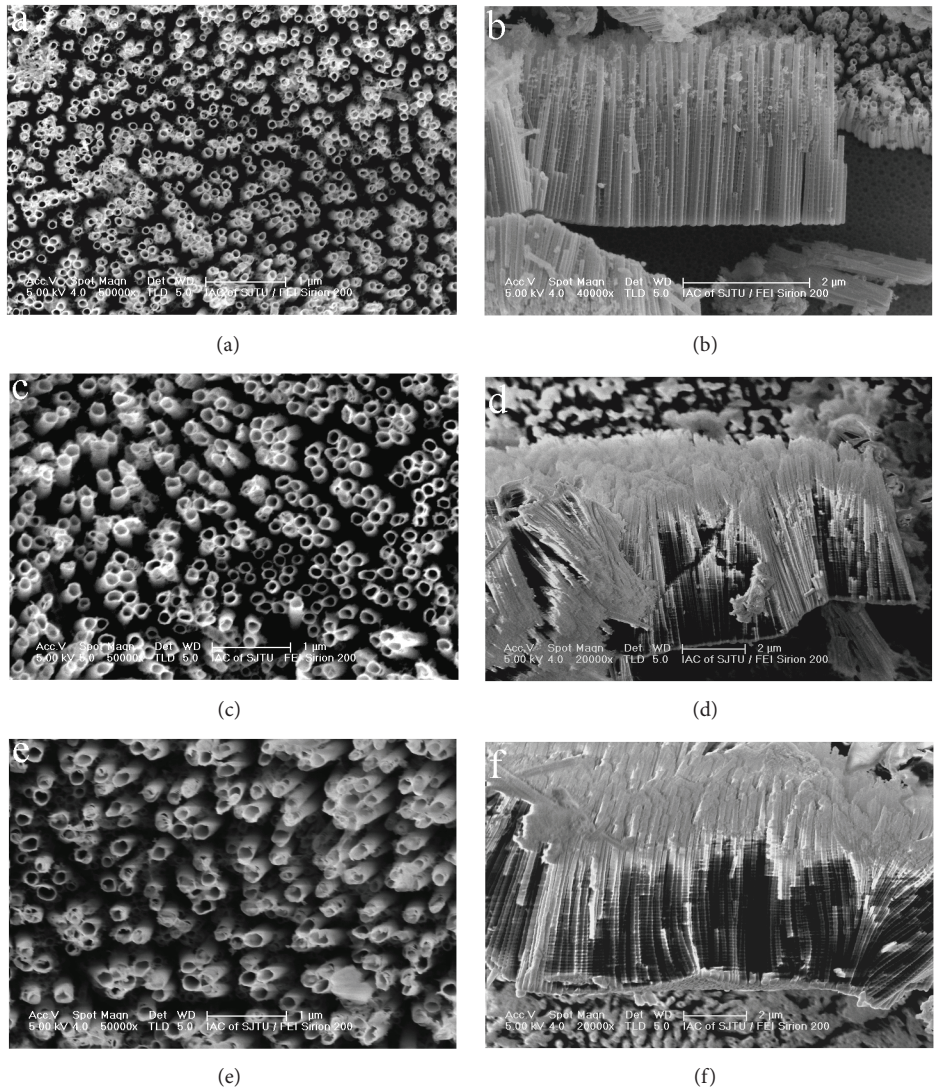

(a) (b) (c) (d) (e) (f)

Figure 3: Top and cross-section views of Ti-Nb-Zr-O nanotubes grown on Ti35Nb15Zr alloy substrate at different voltages with a constant frequency of 4000 Hz and duty cycle of 20% for 90 minutes, (a)-(b) 20 V, (c)-(d) 30 V, and (e)-(f) 40 V.

XRD analyses were conducted to characterize the crystal structure of the as-annealed Ti-Nb-Zr-O oxides with different Zr contents. As shown in Figure 5, diffraction peaks corresponding to the anatase TiO_2 phase in the as-annealed Ti-Nb-Zr-O samples could be found. The (101) diffraction peak of undoped TiO_2 appeared at 2θ value of 25.78°. However, after Nb- and Zr-doping the (101) diffraction peaks of the Ti-Nb-Zr-O samples gradually shifted from 25.78° to 25.05° with increase of the Zr content. This performance should be mainly attributed to the change of TiO_2 lattice parameter because of the larger radius of Zr^{4+} (0.72 Å) compared to that of Ti^{4+} (0.61 Å) [26].

4. Conclusions

In summary, anodic Ti-Nb-Zr-O nanotube arrays were grown on Ti-Nb-Zr alloy substrates in 1 M NaH_2PO_4 containing 0.5 wt% HF electrolytes. The average length of the Ti-Nb-Zr-O nanotubes increased with increase of the Zr content. The anodic current for the Ti-Nb-Zr alloy with higher Zr content was larger than that with lower Zr content at the same anodization voltage. XRD analysis indicated that the Ti-Nb-Zr-O oxides annealed at 500°C were anatase phase. The diffraction peaks shifted to lower 2θ values with increase of the Zr content because of the larger radius of Zr^{4+} compared to that of Ti^{4+}. The formation of Ti-Nb-Zr-O nanotubes for the system with a higher Zr content was relatively easier.

Conflict of Interests

The authors declare that there is no conflict of interests regarding the publication of this paper.

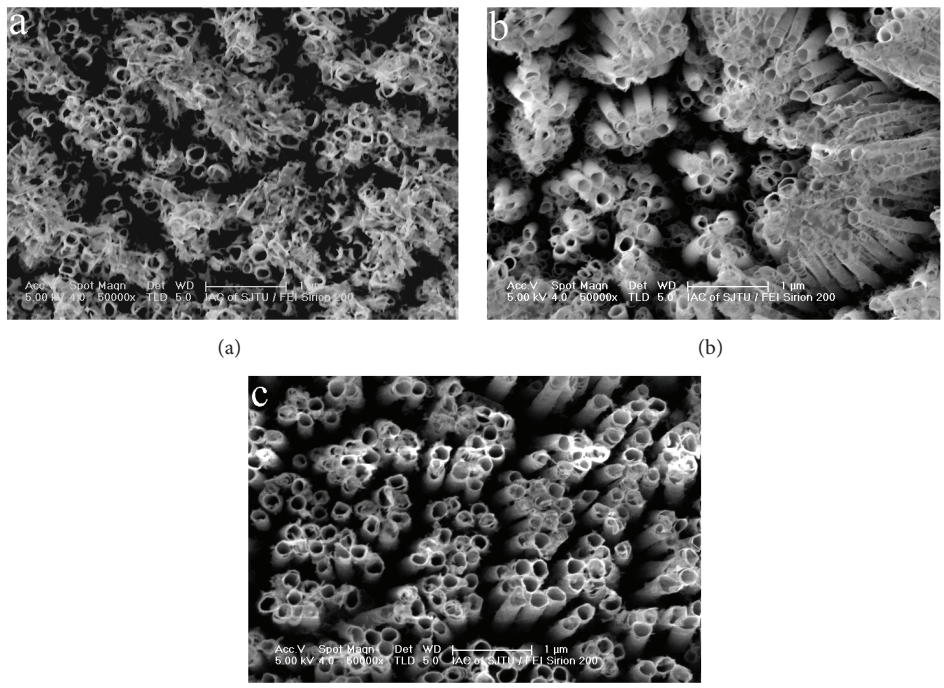

(a) (b)

(c)

Figure 4: SEM images of Ti-Nb-Zr-O nanotubes grown on different Ti-Nb-Zr alloy substrates at 40 V with a constant frequency of 2000 Hz and duty cycle of 20% for 90 minutes, (a) Ti35Nb5Zr, (b) Ti35Nb10Zr, and (c) Ti35Nb15Zr.

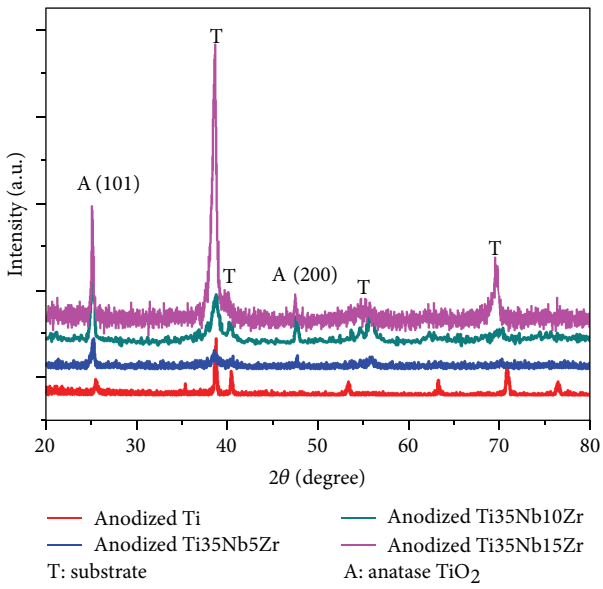

Figure 5: XRD patterns of Ti-Nb-Zr-O nanotubes grown on different Ti-Nb-Zr alloy substrates at 40 V with a constant frequency of 4000 Hz and duty cycle of 20% for 90 minutes.

Acknowledgments

This work was supported by Shanghai Pujiang Program (no. 07pj14047). The authors thank the contribution from SEM Lab at Instrumental Analysis Center of SJTU.

References

[1] H. Kato, K. Asakura, and A. Kudo, "Highly efficient water splitting into H_2 and O_2 over lanthanum-doped $NaTaO_3$ photocatalysts with high crystallinity and surface nanostructure," *Journal of the American Chemical Society*, vol. 125, no. 10, pp. 3082–3089, 2003.

[2] E. Rossinyol, J. Arbiol, F. Peiró et al., "Nanostructured metal oxides synthesized by hard template method for gas sensing applications," *Sensors and Actuators B: Chemical*, vol. 109, no. 1, pp. 57–63, 2005.

[3] X. Fang, Y. Bando, U. K. Gautam, C. Ye, and D. Golberg, "Inorganic semiconductor nanostructures and their field-emission applications," *Journal of Materials Chemistry*, vol. 18, no. 5, pp. 509–522, 2008.

[4] H. Rensmo, K. Keis, H. Lindström et al., "High light-to-energy conversion efficiencies for solar cells based on nanostructured ZnO electrodes," *Journal of Physical Chemistry B*, vol. 101, no. 14, pp. 2598–2601, 1997.

[5] A. Fujishima and K. Honda, "Electrochemical photolysis of water at a semiconductor electrode," *Nature*, vol. 238, no. 5358, pp. 37–38, 1972.

[6] S. In, A. Orlov, R. Berg et al., "Effective visible light-activated B-doped and B,N-codoped TiO_2 photocatalysts," *Journal of the American Chemical Society*, vol. 129, no. 45, pp. 13790–13791, 2007.

[7] F. N. Sayed, O. D. Jayakumar, R. Sasikala et al., "Photochemical hydrogen generation using nitrogen-doped TiO_2–Pd nanoparticles: facile synthesis and effect of Ti^{3+} incorporation," *The Journal of Physical Chemistry C*, vol. 116, pp. 12462–12467, 2012.

[8] K. Nagaveni, M. S. Hegde, and G. Madras, "Structure and photocatalytic activity of $Ti_{1-x}M_xO_{2\delta}$ (M= W, V, Ce, Zr, Fe, and

Cu) synthesized by solution combustion method," *Journal of Physical Chemistry B*, vol. 108, no. 52, pp. 20204–20212, 2004.

[9] M. Hirano and K. Matsushima, "Photoactive and adsorptive niobium-doped anatase (TiO_2) nanoparticles: influence of hydrothermal conditions on their morphology, structure, and properties," *Journal of the American Ceramic Society*, vol. 89, no. 1, pp. 110–117, 2006.

[10] S.-M. Chang and R.-A. Doong, "Characterization of Zr-doped TiO_2 nanocrystals prepared by a nonhydrolytic sol-gel method at high temperatures," *Journal of Physical Chemistry B*, vol. 110, no. 42, pp. 20808–20814, 2006.

[11] H. Zhang, P. Liu, X. Liu et al., "Fabrication of highly ordered TiO_2 nanorod/nanotube adjacent arrays for photoelectrochemical applications," *Langmuir*, vol. 26, no. 13, pp. 11226–11232, 2010.

[12] T. Kasuga, M. Hiramatsu, A. Hoson, T. Sekino, and K. Niihara, "Formation of titanium oxide nanotube," *Langmuir*, vol. 14, no. 12, pp. 3160–3163, 1998.

[13] B. Liu and E. S. Aydil, "Growth of oriented single-crystalline rutile TiO_2 nanorods on transparent conducting substrates for dye-sensitized solar cells," *Journal of the American Chemical Society*, vol. 131, no. 11, pp. 3985–3990, 2009.

[14] C. Ruan, M. Paulose, O. K. Varghese, G. K. Mor, and C. A. Grimes, "Fabrication of highly ordered TiO_2 nanotube arrays using an organic electrolyte," *Journal of Physical Chemistry B*, vol. 109, no. 33, pp. 15754–15759, 2005.

[15] N. K. Allam, A. J. Poncheri, and M. A. El-Sayed, "Vertically oriented Ti-Pd mixed oxynitride nanotube arrays for enhanced photoelectrochemical water splitting," *ACS Nano*, vol. 5, no. 6, pp. 5056–5066, 2011.

[16] F. M. Bayoumi and B. G. Ateya, "Formation of self-organized titania nano-tubes by dealloying and anodic oxidation," *Electrochemistry Communications*, vol. 8, no. 1, pp. 38–44, 2006.

[17] H. Liu, D. Ding, C. Ning, and Z. Li, "Wide-range hydrogen sensing with Nb-doped TiO_2 nanotubes," *Nanotechnology*, vol. 23, no. 1, Article ID 015502, 2012.

[18] N. K. Allam, F. Alamgir, and M. A. El-Sayed, "Enhanced photoassisted water electrolysis using vertically oriented anodically fabricated Ti-Nb-Zr-O mixed oxide nanotube arrays," *ACS Nano*, vol. 4, no. 10, pp. 5819–5826, 2010.

[19] Z. H. Li, C. Q. Ning, D. Y. Ding, H. G. Liu, and L. Huang, "Biological properties of Ti-Nb-Zr-O nanostructures grown on Ti35Nb5Zr alloy," *Journal of Nanomaterials*, vol. 2012, Article ID 834042, 7 pages, 2012.

[20] A. Ghicov and P. Schmuki, "Self-ordering electrochemistry: a review on growth and functionality of TiO_2 nanotubes and other self-aligned MO_x structures," *Chemical Communications*, no. 20, pp. 2791–2808, 2009.

[21] K. Yasuda and P. Schmuki, "Control of morphology and composition of self-organized zirconium titanate nanotubes formed in $(NH_4)_2SO_4/NH_4F$ electrolytes," *Electrochimica Acta*, vol. 52, no. 12, pp. 4053–4061, 2007.

[22] G. Z. Li, H. P. Tang, W. Y. Zhang, G. Li, L. L. Yu, and Y. N. Li, "Fabrication of multilayer Nb_2O_5 nanoporous film by anodization of niobium foils," *Rare Metals*, 2013.

[23] H. Habazaki, M. Uozumi, H. Konno et al., "Influences of structure and composition on growth of anodic oxide films on Ti-Zr alloys," *Electrochimica Acta*, vol. 48, no. 20-22, pp. 3257–3266, 2003.

[24] H. Tsuchiya, J. M. MacAk, A. Ghicov, L. Taveira, and P. Schmuki, "Self-organized porous TiO_2 and ZrO_2 produced by anodization," *Corrosion Science*, vol. 47, no. 12, pp. 3324–3335, 2005.

[25] X. J. Feng, J. M. Macak, S. P. Albu, and P. Schmuki, "Electrochemical formation of self-organized anodic nanotube coating on Ti-28Zr-8Nb biomedical alloy surface," *Acta Biomaterialia*, vol. 4, no. 2, pp. 318–323, 2008.

[26] X. Lü, X. Mou, J. Wu et al., "Improved-performance dye-sensitized solar cells using Nb-doped TiO_2 electrodes: efficient electron injection and transfer," *Advanced Functional Materials*, vol. 20, no. 3, pp. 509–515, 2010.